

# **Imaging Plasmon Hybridization of Fano Resonances via Hot-Electron-Mediated Absorption Mapping**

Sabrina Simoncelli<sup>1,2‡\*</sup>, Yi Li<sup>1‡</sup>, Emiliano Cortés<sup>1\*</sup> and Stefan A. Maier<sup>1,3</sup>

<sup>1</sup>*The Blackett Laboratory, Department of Physics, Imperial College London, London SW7 2AZ, United Kingdom*

<sup>2</sup>*Department of Physics and Randall Division of Cell and Molecular Biophysics, King's College London, London SE1 1UL, United Kingdom*

<sup>3</sup>*Chair in Hybrid Nanosystems, Nanoinstitut Munich, Faculty of Physics, Ludwig-Maximilians-Universität München, 80799 München, Germany.*

<sup>‡</sup>*These authors contributed equally to this work*

\* Email: [s.simoncelli@imperial.ac.uk](mailto:s.simoncelli@imperial.ac.uk), [e.cortes@imperial.ac.uk](mailto:e.cortes@imperial.ac.uk)

## **Contents**

- S1. Gold nanostructures fabrication
- S2. Scanning electron microscopy (SEM) imaging
- S3. Dark-field scattering spectroscopy
- S4. Gold antennas-DNA functionalization
- S5. Fluorescence microscopy imaging
- S6. Super-resolution data processing and image analysis
- S7. Femtosecond pulsed-laser irradiation
- S8. Numerical simulations

### Supporting Figures

- Fig. S1. Scattering spectra of gold Fano nanostructures.
- Fig. S2. Super resolution m-PAINT imaging of gold nanostructures.
- Fig. S3. Localization precision and cross-sectional histograms.
- Fig. S4. Polarized m-PAINT images and calculated total fluorescence enhancements.
- Fig. S5. Examples of power-dependent absorption maps.
- Fig. S6. Example of calculated absorption maps considering both: resistive losses and dye-antenna coupling effect.
- Fig. S7. Scattering spectra of gold Fano nanostructures with varying gap sizes.
- Fig. S8. Super resolution m-PAINT imaging of the un-coupled gold Fano nanostructures.
- Fig. S9. Plasmonic response of the un-coupled Fano structure.

### Supporting References

## **S1. Gold nanostructures fabrication**

Arrays of gold nanoantennas were fabricated on borosilicate glass coverslips using electron beam lithography (E-line, Raith GmbH). First, the substrate was spin-coated with a positive tone resist, poly(methyl methacrylate) (PMMA 950K A4, Microchem), and baked for at least 3 min at 180 °C. Then, a conductive layer of Espacer 300Z (Showa Denko) was spin coated onto the sample. The substrate was exposed with an electron beam at 20 keV followed by a methyl isobutyl ketone (MIBK) / isopropanol (1:3) based development procedure. The nanostructured PMMA was then cleaned by a plasma ash etch step (Femto, Diener Electronic GmbH, 7 s at 40 % power) and covered with a 1.5 nm chromium layer and a 40 nm gold layer deposited *via* thermal evaporation (Amod, Angstrom Engineering Inc, 1.5 Å/s rate). The fabrication process was completed with a standard lift-off process using Remover 1165 (Microposit, Dow Electronic Materials) at 70 °C.

## **S2. Scanning electron microscopy (SEM) imaging**

Gold nanoantennas were imaged in an E-line Raith microscope (Raith GmbH). Prior to SEM imaging, a 20-nm thin film of Espacer 300Z was coated onto the sample (2,000 r.p.m., 60 s) followed by a 60 s, 90 °C baking step. Imaging was performed with an electron acceleration voltage of 10 keV, a beam aperture of 30 µm and a working distance of 10 mm.

## **S3. Dark-field scattering spectroscopy**

Single-particle dark-field scattering spectra were acquired in air using an upright Nikon Eclipse Ti-U microscope (Nikon Instruments) equipped with a dark field objective (Nikon LU Plan ELWD 100× NA 0.80), which is used for both, to provide the incident illumination and to collect the scattered light. For illumination, a 100 W halogen lamp (Nikon) was used. The scattered light was measured with a diffractive grating and charge-coupled device camera cooled to 70 K. The plotted spectra are corrected for the system wavelength response (by measuring the cross section of a perfect reference white rough scatter) and also for dark and background counts.

## **S4. Gold antennas-DNA functionalization**

Gold nanoantenna arrays supported on borosilicate glass coverslips were first thoroughly cleaned with isopropanol and water, dried with nitrogen and left for 1.5 min in a UVO cleaner/oxidizer (Femto, Diener Electronic GmbH). The sample was mounted to a bottomless self-adhesive slide (sticky-Slide VI 0.4, Ibidi) which, has been previously plasma clean for 10 min, to

form a flow chamber of six individual channels with inner volumes of  $\sim 30 \mu\text{L}$  each. Each channel was functionalized with the single stranded DNA docking strand, ThiolC6-SpacerC18-ATGAGTTAATT (biomers.net GmbH), independently from the other. First, the docking strand was reduced by incubating  $20 \mu\text{L}$  of  $100 \mu\text{M}$  thiolated DNA with  $20 \mu\text{L}$  of freshly prepared  $10 \text{ mM}$  (Tris (carboxyethyl) phosphine hydrochloride (TCEP, Sigma Aldrich) solution for 30 minutes at room temperature. Then,  $1 \mu\text{M}$  of the activated thiol-labeled ssDNA oligo diluted in  $10 \text{ mM TRIS-HCl}$ ,  $1 \text{ M NaCl}$ ,  $\text{pH} = 7$  (buffer A) was flown into the channel and incubated overnight in the dark, at room temperature. The next day, the channel was washed with  $100 \mu\text{L}$  of buffer A and a solution of  $1 \text{ mM}$  6-Mercapto-1-hexanol (MCH, Sigma Aldrich) was flown and incubated for 30 minutes at room temperature. Finally, the sample was left in either  $10 \text{ mM TRIS-HCl}$ ,  $50 \text{ mM NaCl}$ ,  $\text{pH} = 7$  (buffer B) or  $5 \text{ mM TRIS-HCl}$ ,  $10 \text{ mM MgCl}_2$ ,  $1 \text{ mM EDTA}$ ,  $\text{pH} = 8$  (buffer C) for femtosecond pulsed-laser irradiation or fluorescence imaging, respectively, after washing it with  $100 \mu\text{L}$  of buffer B. For fluorescence microscopy imaging, a solution of the imager strand, Atto655-TTAACTCATG-3' (biomers.net GmbH), diluted to the desired concentration in buffer C was flown into the channel immediately before starting the measurements. To estimate the surface coverage of the mix monolayer (MCH + thiolated-DNA docking strand) we performed reductive electrodesorption measurements on polycrystalline preferred oriented Au (111) electrodes as described in Supporting Reference S1.<sup>1</sup> While the coverage of the mix monolayer is the maximum surface coverage reached by thiolate species on Au surfaces,  $\theta \approx 1/3$ , the ratio of MCH/ss-DNA molecules in our mix monolayer is in the order of  $\sim 160$  to 1.

## **S5. Fluorescence microscopy imaging**

Total internal reflection fluorescence (TIRF) imaging experiments were conducted in a custom-built TIRF set-up based on an inverted Nikon Eclipse Ti-U microscope (Nikon Instruments) and a  $647 \text{ nm}$  CW laser (OBIS LX 120mW, Coherent) spectrally filtered with a clean-up filter (BrightLine FF 640/20-25, Semrock). A single-edge dichroic beam splitter (BrightLine FF 649, Semrock) was used to reflect the excitation light into the oil immersion TIRF objective (Apo DIC N2 TIRF 100 $\times$ , numerical aperture (NA) 1.49, oil). Fluorescence light was passed through an emission filter (ET705/72m, Chroma Technology) and collected on an electron-multiplying charge-coupled device (EMCCD) camera (Evolve 512 Delta, Photometrics), with an effective pixel size of  $160 \text{ nm}$ . For metallic DNA-PAINT measurements, 40,000 frames per super-resolution image were recorded at a frame rate of 33Hz and at an excitation density of  $\sim 850 \text{ W cm}^{-2}$ . The CCD readout bandwidth was set to  $5 \text{ MHz}$  at 16 bits and 3 pre-amp gain. The electron multiplying (EM) gain was set at 200.

The concentration of the imager strand was 0.5 nM and it was determined empirically to guarantee binding of only one single imager strand per diffraction limited-area.

## **S6. Super-resolution data processing and image analysis**

Stage drift correction was performed using a subpixel image registration algorithm based on cross-correlation (single-step DFT algorithm, Supporting Reference S2)<sup>2</sup>. Prior single molecule localization, the static gold luminescence background from the gold nanoantennas was subtracted by generating an average image of the drift-corrected image stack with an in-house Matlab routine. Precise localization of the fluorescent single molecule imager-docking binding events diffraction limited spots was performed by Gaussian fitting with the rainSTORM Matlab application presented in Supporting Reference S3.<sup>3</sup> m-PAIN images of individual gold Fano nanoantennas were typically reconstructed from ~ 1000 to 6,000 localizations. Particle averaging of gold nanoantennas exposed to specific chemical and/or optical conditions was performed using a translation registration algorithm (Matlab built-in function), which estimates the geometric transformation that aligns an image with a fixed template. The template was design according to the shape and dimension of each type of fabricated nanoantenna. Average m-PAIN images were usually reconstructed by overlying super-resolution images of 30 to 36 individual gold nanoantennas that had been exposed to the same conditions.

## **S7. Femtosecond pulsed-laser irradiation.**

We adapted a Nikon Eclipse Ti-U microscope (Nikon Instruments) for single-particle femtosecond pulsed-laser irradiation by coupling a collinear optical parametric amplifier (ORPHEUS, Light Conversion Ltd.) with a LYRA wavelength extension option (Light Conversion Ltd., pulse duration of 180 fs, repetition rate of 100 kHz) pumped by a femtosecond Ytterbium based laser system (PHAROS, Light Conversion Ltd.). The excitation beam was set either to 750, 820 or 953 nm and reflected by a beam splitter (BSS11R, Thorlabs) or by dichroic mirror short-pass dichroic mirror (DMSP805, Thorlabs) and focused onto the sample with a 40× (CFI S Plan Fluor ELWD 40×, NA 0.60) air objective from Nikon. The beam polarization was adjusted with a half-wave plate and a polarizer. The sample was fixed to an XYZ piezo-scanner stage (Nano-Drive, Mad City Laboratories), which allows automatic single nanoantenna irradiation. Each nanoantenna was irradiated for 10 seconds at different power densities as described in Figure 5 of the main text. Following irradiation, a washing step consisting of at least three washes using 100 µL of buffer B was performed. Alignment of the antennas with the excitation beam was possible by inspecting the

sample with white light illumination and detecting the sample using a CCD camera (QICAM Fast 1394, QImaging).

## S8. Numerical simulations.

Optical scattering and absorption performances of gold Fano nanoantenna of bar and disks were examined using commercial software Lumerical FDTD v2017a. The dielectric functions of Au and Cr were extracted from the data of Johnson and Christy<sup>4</sup> and Palik<sup>5</sup>, respectively. Total-field scattered-field (TFSF) source was used to study the scattering performance of individual nanoantennas. The calculated Fano interference in air matches well with the previous work in our group.<sup>6</sup> The charge distributions within metals were associated with specified wavelengths. The power absorption per unit volume due to material absorption was then calculated using the built-in advanced method, which minimizes interpolation errors that occur due to discontinuities in the electric field near interfaces. (<http://kb.lumerical.com/en/index.html>)

To interpret the local density of states (LDOS) coupled with our plasmonic Fano system, Green's function analysis was used to calculate the emission enhancement  $(\phi/\phi^0)_f$  of a single dipole emitter at 655 nm wavelength located in the vicinity of the gold Fano antenna. The emitter was oriented either along  $x$ ,  $y$  or  $z$  axis, respectively. We then move the dipole position with a step size of 5 nm over a scanning region of  $200 \times 200 \text{ nm}^2$  where the center of the nanoantenna is aligned at the original  $(0, 0)$  point. During all the calculations, the height of the dipole source is fixed at  $z = 7$  nm above the gold surface in order to match with our experimental conditions. The new quantum efficiency  $\phi$  was calculated as  $\frac{\gamma_r/\gamma_0}{1-\phi_{fl} + \gamma_r/\gamma_0 + \gamma_{nr}/\gamma_0}$  using the same method from three different research groups<sup>7-9</sup>, where the quantum yield  $\phi_{fl}$  of Atto655 ([www.atto-tec.com](http://www.atto-tec.com)) is set as 30%. Since the excitation enhancement  $(\gamma/\gamma^0)_{exc}$  is derived from the electromagnetic near-field distribution at 640 nm wavelength, the total fluorescent enhancement becomes  $(\gamma/\gamma^0)_{exc}(\phi/\phi^0)_f$ .

## Supporting Figures

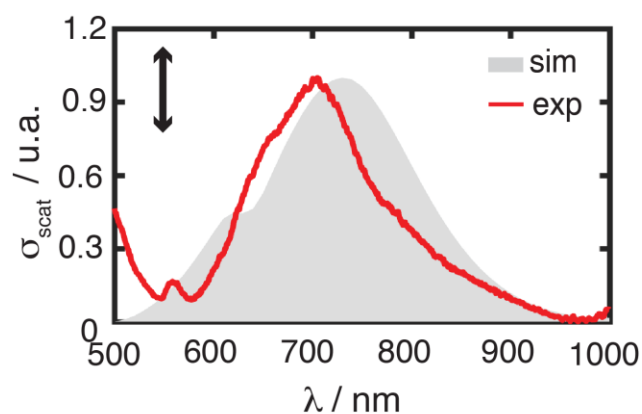


**Figure S1. Scattering spectra of gold Fano nanostructures.** FDTD-simulated (grey area) and measured (red line) single-antenna scattering spectra of the Fano structure composed of two 160 nm in diameter disk close to a  $340 \times 80 \text{ nm}^2$  bar in air for perpendicular ( $90^\circ$ ) polarized illumination. The gap size between the bar and the disks is 20 nm.

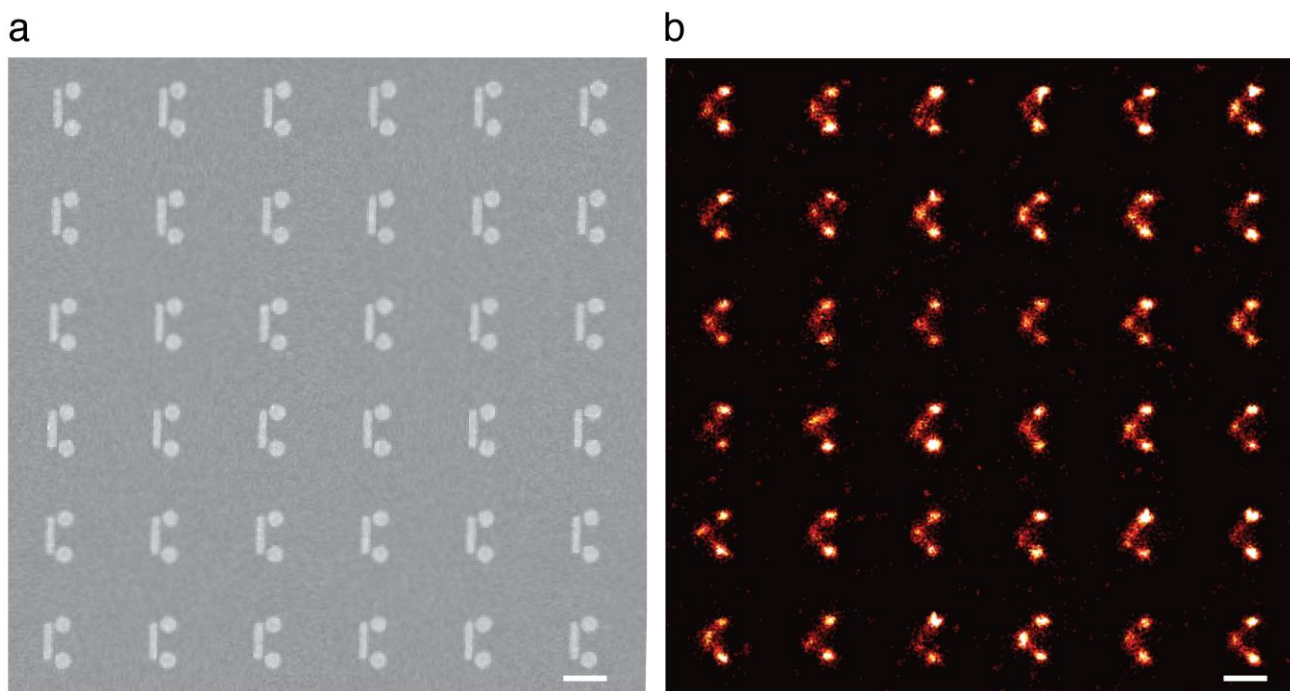


**Figure S2. Super resolution m-PAINt imaging of gold Fano nanostructures.** a, SEM and b, super-resolved metallic DNA-PAINt image of a  $6 \times 6$  array of individual Fano nano-sized gold structures fabricated with electron beam lithography. m-PAINt movie was collected using 0.5 nM concentration of imager strand in imaging buffer C. The scale bar corresponds to 400 nm.

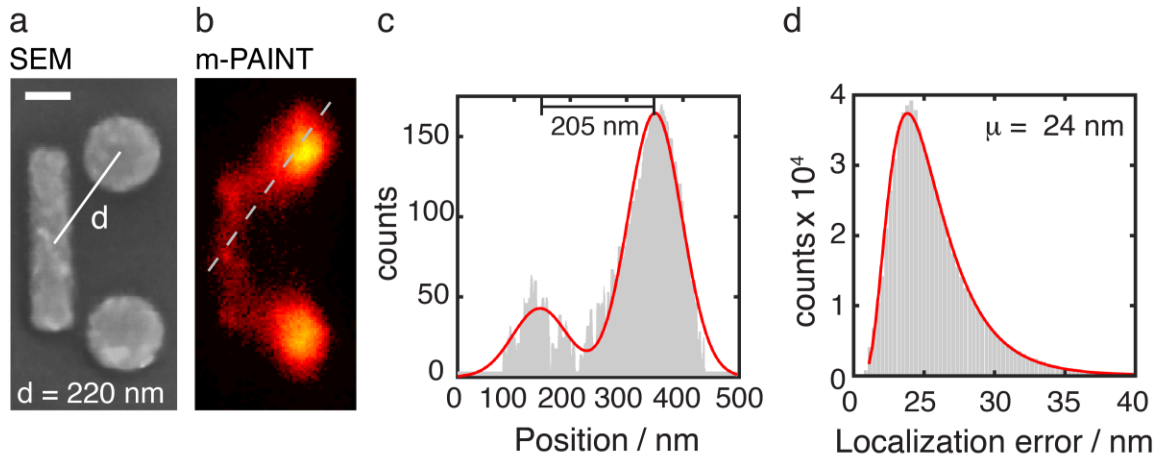


**Figure S3. Localization precision and cross-sectional histograms.** **a**, SEM and **b**, average super-resolved metallic DNA-PAINT image of 35 individual gold Fano nanostructures of dimensions  $340 \times 80 \text{ nm}^2$  (bar) and  $160 \text{ nm}$  (disks). **c**, Cross-sectional histogram along the dashed line in **b** revealing a distance of  $\sim 205 \text{ nm}$  closed to the SEM confirmed distance of  $\sim 220 \text{ nm}$ . **d**, Histogram of the error in the localization of single molecule events. The scale bar corresponds to  $100 \text{ nm}$ .

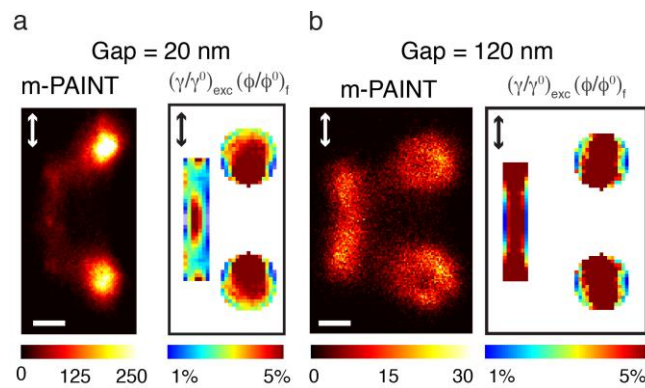


**Figure S4. Polarized m-PAINT images and calculated total fluorescence enhancements.** Average super-resolved m-PAINT image of 36 individual gold Fano nanostructures of dimensions  $340 \times 80 \text{ nm}^2$  (bar) and  $160 \text{ nm}$  (disks) in the left panel, together with total fluorescence enhancement  $(\gamma/\gamma^0)_{exc}(\phi/\phi^0)_f$  in the right panel for a gap of  $20 \text{ nm}$  (**a**) or  $120 \text{ nm}$  (**b**). The mean number of localizations in individual images is  $6,500 \pm 1,600$  (**a**) and  $1100 \pm 400$  (**b**). Fluorescence excitation was performed with a linearly polarized laser of  $647 \text{ nm}$  polarized along the longer axis of the nano-sized bar. The scale bar corresponds to  $100 \text{ nm}$ . For all the super-resolution images presented in this manuscript the same docking strands have been employed, ensuring the same distance between the dye and the antenna for all the cases.

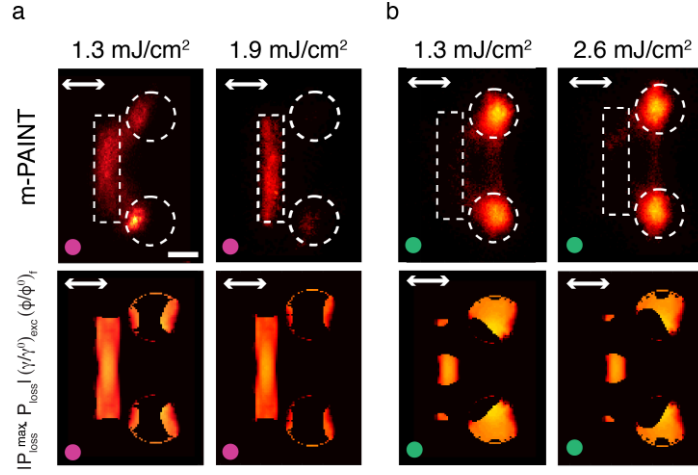


**Figure S5. Examples of power-dependent absorption maps.** *Top:* Average super-resolved m-PAINT images of 32 to 35 individual gold Fano nanostructures of dimensions  $340 \times 80 \text{ nm}^2$  (bar) and 160 nm (disks) after irradiation with a 750 nm (violet, a) and 935 nm (green, Fano resonance, b) linearly polarized femtosecond pulsed laser of  $1.3 \text{ mJ/cm}^2$  or  $1.8 \text{ mJ/cm}^2$  (750 nm) or  $2.6 \text{ mJ/cm}^2$  (935 nm) fluence. The mean number of localizations in individual images from left to right is  $2,800 \pm 400$ ;  $2,100 \pm 500$ ;  $4,300 \pm 800$  and  $4,100 \pm 1,100$ . Fluorescence excitation was performed with a linearly polarized 647 nm laser polarized along the longer axis of the nano-sized bar. *Bottom:* FDTD-calculated absorption map distribution considering both resistive losses and dye-antenna coupling effect calculated as detailed in Figure S5 for a single Fano antenna illuminated in water at 750 nm (violet) and 935 nm (green, Fano resonance). White arrows represent the polarization of the incident light. The scale bar corresponds to 100 nm.

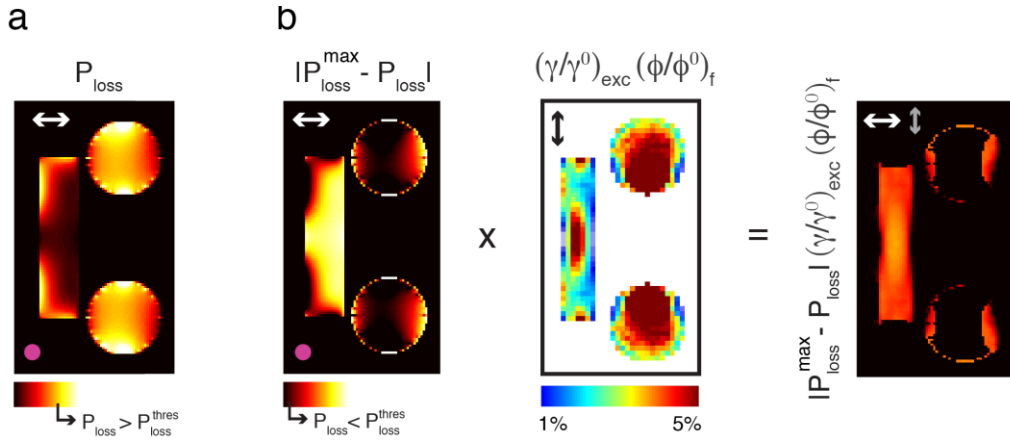


**Figure S6. Example of calculated absorption maps considering both: resistive losses and dye-antenna coupling effect.** **a**, FDTD-calculated resistive losses distribution,  $P_{\text{loss}}$ , of a single Fano structure of dimensions  $340 \times 80 \text{ nm}^2$  (bar) and 160 nm (disks) with a 20 nm gap illuminated in water with parallel ( $0^\circ$ ) polarized illumination at 750 nm. **b**, FDTD-calculated complementary resistive losses distribution for the same conditions as in **(a)** (*left*), calculated total fluorescence enhancement distribution  $(\gamma/\gamma^0)_{\text{exc}}(\phi/\phi^0)_f$  under linearly polarized fluorescence excitation ( $\lambda_{\text{exc}} = 647 \text{ nm}$ ) along the longer axis of the nano-sized bar (*middle*), and calculated absorption distribution obtained by multiplying the complementary resistive losses and total fluorescence enhancement maps (*right*). Arrows represent the polarization of the incident light. The complementary resistive losses maps



were calculated by subtracting the maximum resistive losses value out of the six different conditions (3 wavelengths, and 2 irradiation polarizations),  $P_{loss}^{max}$ , to each of the resistive losses maps:  $|P_{loss}^{max} - P_{loss}|$ . For the final calculated absorption distribution maps all the regions with resistive losses higher than a threshold of resistive losses for thiol-desorption,  $P_{loss}^{thres}$ , of  $2 \mu\text{W}/\text{nm}^3$  were considered as null values.

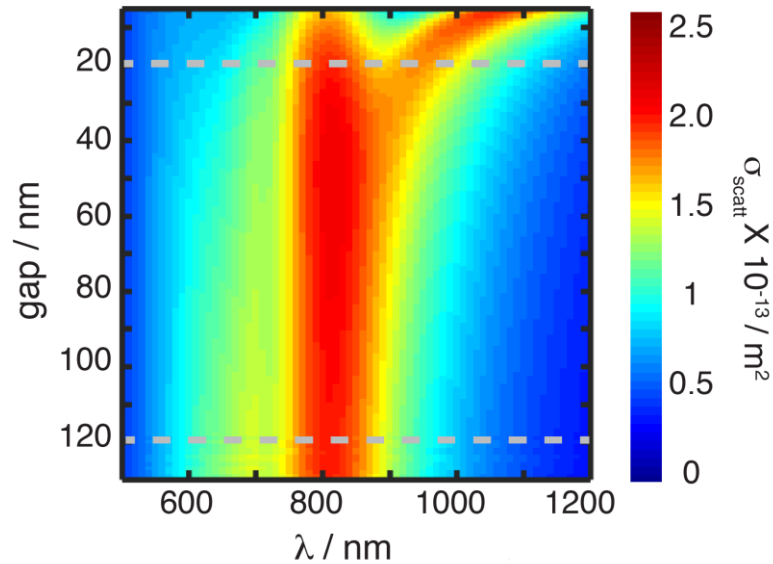


**Figure S7. Scattering spectra of gold Fano nanostructures with varying gap sizes.** Scattering cross-sections calculated by FDTD for a single gold Fano structure of dimensions  $340 \times 80 \text{ nm}^2$  (bar) and 160 nm (disks) in water for parallel ( $0^\circ$ ) polarized illumination as function of the gap size between the bar and the disks.

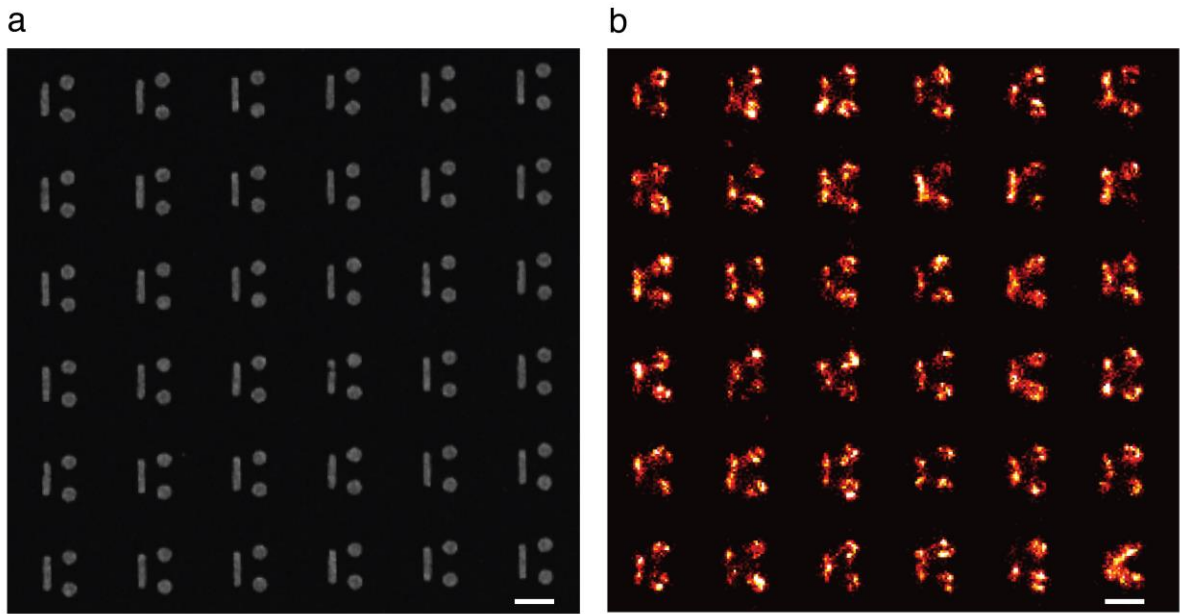


**Figure S8. Super resolution m-PAINt imaging of the un-coupled gold Fano nanostructures.** **a**, SEM and **b**, super-resolved metallic DNA-PAINt image of a 6×6 array of individual un-coupled Fano nano-sized gold structures fabricated with electron beam lithography. m-PAINt movie was collected using 0.5 nM concentration of imager strand in imaging buffer C. The scale bar corresponds to 400 nm.

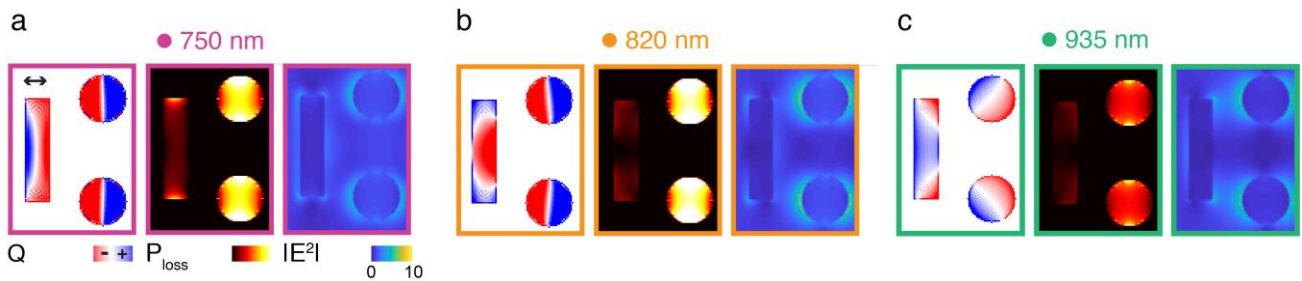


**Figure S9. Plasmonic response of the un-coupled Fano structure.** FDTD-calculated charge density (left),  $Q$ , resistive losses (middle),  $P_{loss}$ , and electrical-field (right),  $E^2$ , distribution of a single Fano structure of dimensions  $340 \times 80 \text{ nm}^2$  (bar) and 160 nm (disks) and gap of 120 nm illuminated in water at (a) 750 nm, (b) 820 nm and (c) 935 nm for parallel ( $0^\circ$ ) polarized illumination.

### Supporting References

- (S1) Simoncelli, S.; Li, Y.; Cortés, E.; Maier, S. A. *ACS Nano* **2018**, *12*, 2184–2192.
- (S2) Guizar-Sicairos, M.; Thurman, S. T.; Fienup, J. R. *Opt. Lett.* **2008**, *33*, 156–158.
- (S3) Rees, E. J.; Erdelyi, M.; Pinotsi, D.; Knight, A.; Metcalf, D.; Kaminski, C. F. *Opt. Nanoscopy* **2012**, *1*, 12.
- (S4) Johnson, P. B.; Christy, R. W. *Phys. Rev. B* **1972**, *6*, 4370–4379.
- (S5) Palik, E. *Handbook of Optical Constants of Solids*; 1998.
- (S6) Gennaro, S. D.; Rahmani, M.; Giannini, V.; Aouani, H.; Sidiropoulos, T.; Cia, M. N.-; Maier, S. A.; Oulton, R. F. *Nano Lett.* **2016**, *16*, 5278–5285.
- (S7) Estrada, L. C. C.; Roberti, M. J. J.; Simoncelli, S.; Levi, V.; Aramendía, P. F. F.; Martínez, O. E. E. *J. Phys. Chem. B* **2012**, *116*, 2306–2313.
- (S8) Mack, D. L.; Cortés, E.; Giannini, V.; Török, P.; Roschuk, T.; Maier, S. A. *Nat. Commun.* **2017**, *8*, 14513.
- (S9) Cheng, Y.; Stakenborg, T.; Van Dorpe, P.; Lagae, L.; Wang, M.; Chen, H.; Borghs, G. *Anal. Chem.* **2011**, *83*, 1307–1314.